


# Multiwavelength Regression Algorithm for Eliminating Chamber Surface Effects of Microfluidic Chips

Applied Spectroscopy  
2019, Vol. 73(1) 40–46  
© The Author(s) 2018  
Article reuse guidelines:  
sagepub.com/journals-permissions  
DOI: 10.1177/0003702818798044  
journals.sagepub.com/home/asp  


Yang Xu<sup>1,2</sup> , Yihui Wu<sup>1</sup>, JunFeng Wu<sup>1</sup>, and Mingbo Chi<sup>1</sup> 

## Abstract

An ultraviolet visible (UV–Vis) spectrophotometric and multiwavelength linear regression (MLR) method was developed for eliminating the influence of the surface quality of centrifugal microfluidic chips on the accuracy of their absorbance detection. The regression model is based on scalar scattering theory. The method was validated with cuvettes with different surface quality and Orange G (orange gelb) dye. The coefficients of variation (CVs) of the predicted solution concentration ratios in different cuvettes were < 1%, and the relative errors were < 1.5%. The model was shown to have higher accuracy and precision than that of traditional methods.

## Keywords

Ultraviolet–visible, UV–Vis spectrophotometry, multiwavelength linear regression, MLR, centrifugal microfluidic chip, surface roughness

Date received: 27 February 2018; accepted: 2 August 2018

## Introduction

An automatic, centrifugal, microfluidic chip analysis system can carry out fluidic processing such as separation, quantitation, mixing, and transportation of whole blood by implementing different spinning profiles.<sup>1</sup> The process is easy to integrate and can realize fully automated, high-throughput, rapid detection, and have been widely used in biomedical diagnostics, especially in vitro diagnostics (IVD). The Abaxis whole blood analyzer has been widely used in human and animal blood biochemical detections.<sup>2</sup> Samsung has developed an automatic immunoassay system;<sup>3</sup> Changchun Institute of Optics, Fine Mechanics and Physics, Chinese Academy of Sciences (CIOMP) and other organizations have also introduced related prototypes and products.

Quantitative detection by these systems is normally achieved via the double-beam absorbance method based on Beer–Lambert law.<sup>4</sup> In traditional double-beam spectrophotometers, the cuvettes need to be matched to ensure accurate blank readings. According to the cuvette standard of the People's Republic of China (GB/T 26791-2011), the transmittance difference between matched cuvettes should be  $\leq 0.5\%$ . Arrayed chambers are manufactured on centrifugal microfluidic chips by batch manufacture, such as injection molding, and cannot be matched as pairs.

As shown in Fig. 1, ensuring the same quality of multiple surfaces on a single chip is difficult, especially for high-throughput chips. For example, the root mean square (RMS) surface roughness of the bottom surfaces of different chambers on the chip in Fig. 1 differ. Simultaneously, mold wear during the injection molding process will decrease the surface quality of chips. According to the scalar scattering formula, an RMS difference of 20 nm at poly(methyl methacrylate) (PMMA)–air interfaces will result in a transmittance difference > 2% at a wavelength of 440 nm.

In the present work, to eliminate the effect of chamber surface quality on the accuracy of double-beam absorbance detection, a multiwavelength method with a linear expression of the absorbance caused by interface scattering is proposed. The accuracy of this model was verified with cuvettes with different surface qualities. The results show that this model fits well with samples with different concentration.

<sup>1</sup>State Key Laboratory of Applied Optics, Changchun Institute of Optics, Fine Mechanics and Physics, Chinese Academy of Sciences, Changchun, China

<sup>2</sup>University of Chinese Academy of Sciences, Beijing, China

## Corresponding author:

Yihui Wu, No. 3888 Dong Nanhu Road, Changchun, Jilin 130033, China.  
Email: yihuiwu@ciomp.ac.cn

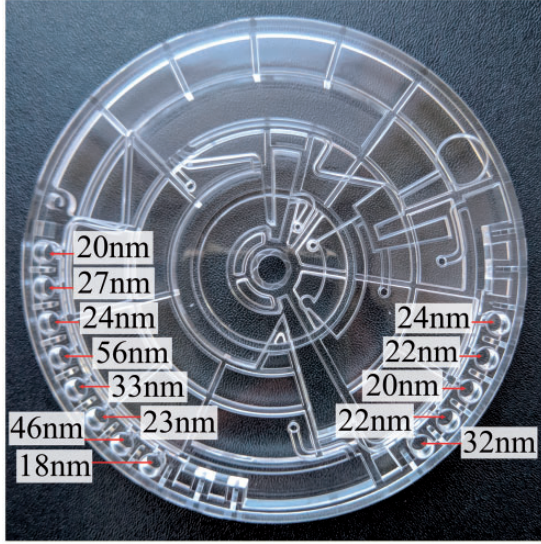


**Figure 1.** Requirements of the bottom surfaces of different chambers on the same chip manufactured by injection molding.

## Theory

According to SPI mold polishing standards, the polished surface roughness  $R_a$  should be  $\leq 5.84 \mu\text{m}$ . The surface topography of microfluidic chips manufactured in a polished mold is well approximate by a Gaussian function.<sup>5,6</sup> Because the distance between the position of the detector aperture stop and the scattering surface is large compared with the wavelength, for the normal incidence of light, the diffusely transmitted light is given by<sup>7</sup>

$$S_T = T_0 \left\{ 1 - \exp \left[ - \left( \frac{2\pi\sigma(n_1 - n_0)}{\lambda} \right)^2 \right] \right\} \times \left\{ 1 - \exp \left[ -2 \left( \frac{\pi l}{\lambda} \right)^2 \right] \right\} \quad (1)$$

where  $\sigma$ ,  $l$ ,  $\lambda$ ,  $n_1$ , and  $n_0$  are the RMS, the autocovariance length, wavelength, refractive index of the incident medium, and refractive index of the refractive medium, respectively. Parameter  $T_0$  is the transmittance of the smooth surface:  $T_0 = \frac{4n_1n_0}{(n_1+n_0)^2}$ .

For well-polished optical surfaces, the autocovariance length  $l$  is much greater than the wavelength.<sup>8</sup> The light intensity received by the detector in the transmission direction is roughly the ideal transmitted light intensity minus the scattered light intensity. To combine the transmittance with the law of absorption, the transmittance is expressed as absorbance:

$$A = \log_{10} \left( \frac{1}{T_0 - S_T} \right) = a_0 + \frac{a_1}{\lambda^2} \quad (2)$$

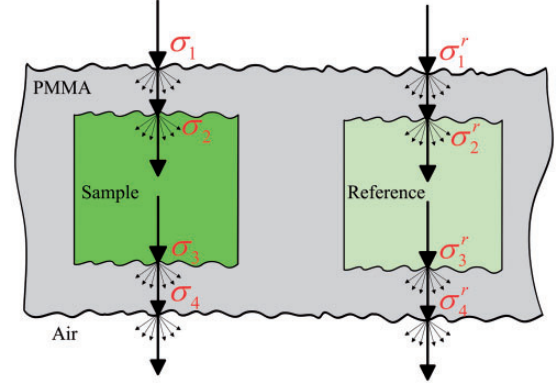


**Figure 2.** Double-beam absorbance detection model of a PMMA microfluidic chip.

where  $a_0 = -\log_{10}(T_0)$  and  $a_1 = \frac{[2\pi\sigma(n_1 - n_0)]^2}{\log_e 10}$ .

The double-beam absorbance detection model of a PMMA microfluidic chip is shown in Fig. 2, where the roughness parameter values differ.

According to the absorbency additivity, the absorbance of the sample chamber and the reference chamber can be expressed as

$$A_s = \sum_{i=1}^4 A_{\sigma_i} + \epsilon_{pmma} c_{pmma} l_{pmma} + \epsilon_{ref} c_{ref} l_{ref} + \epsilon_{tar} c_{tar} l_{tar} \quad (3)$$

$$A_R = \sum_{i=1}^4 A_{\sigma_i^r} + \epsilon_{pmma}^r c_{pmma}^r l_{pmma}^r + \epsilon_{ref}^r c_{ref}^r l_{ref}^r \quad (4)$$

where  $A_{\sigma_1}$ ,  $A_{\sigma_i}$ ,  $c_{pmma}$ ,  $c_{ref}^r$ ,  $l_{pmma}$ , and  $l_{ref}^r$  are the surface absorbance, PMMA molar concentration, and the PMMA path length of the sample chamber and the reference chamber, respectively;  $c_{ref}$ ,  $c_{tar}$ ,  $l_{ref}$ , and  $l_{tar}$  are the molar concentration and the path length of the reference substance and the target substance in the sample;  $c_{ref}^r$  and  $l_{ref}^r$  are molar concentration and path length of the reference substance in the reference chamber, respectively;  $\epsilon_{pmma}$ ,  $\epsilon_{ref}$ , and  $\epsilon_{tar}$  are the molar absorptivity of PMMA, the reference substance, and the target substance, respectively.

The molar absorptivity of PMMA and the target substance can be obtained by measuring an empty chamber and a chamber filled with a standard solution of the target substance, respectively. They can be expressed as

$$\epsilon_{pmma} = \left( A_E - \sum_{i=1}^4 A_{\sigma_i^e} \right) / C_{pmma}^e l_{pmma}^e \quad (5)$$

$$\epsilon_{tar} = \left( A_T - \sum_{i=1}^4 A_{\sigma_i^t} - \epsilon_{pmma} c_{pmma}^t l_{pmma}^t \right) / C_{tar}^t l_{tar}^t \quad (6)$$

where  $A_E$ ,  $A_T$ ,  $A_{\sigma_i^e}$ ,  $A_{\sigma_i^t}$ ,  $C_{pmma}^e$ ,  $C_{pmma}^t$ ,  $l_{pmma}^e$ , and  $l_{pmma}^t$  are the total absorbance, surface absorbance, PMMA molar concentration, PMMA path length of the empty chamber, and standard solution chamber, respectively;  $c_{ref}^t$ ,  $c_{tar}^t$ ,  $l_{ref}^t$  and  $l_{tar}^t$  are the molar concentration, and path length of the reference substance and target substance in the standard solution, respectively.

Substituting Eqs. 2, 4, 5, and 6 into Eq. 3 gives the absorbance of the sample chamber:

$$A_s = c_0 + c_1 \frac{1}{\lambda_2} = c_2 A_E + c_3 A_R + c_4 A_T \quad (7)$$

where  $c_0$ ,  $c_1$ ,  $c_2$ ,  $c_3$ , and  $c_4$  are coefficients related to the parameters of the chambers and solutions (e.g.,  $c_{pmma}^e$ ,  $c_{pmma}^t$ ,  $l_{pmma}^e$  and  $l_{pmma}^t$ ).

The refractive index changes with wavelength. For example, the refractive indexes of PMMA are 1.4966 and 1.4858 at wavelengths of 500 and 800 nm, respectively—a difference of 0.73%. The variation can be ignored here. Thus, a matrix representation of the sample chamber absorbency at  $n$  wavelengths can be obtained:

$$\begin{bmatrix} 1 & \frac{1}{\lambda_1^2} & A_{E-\lambda_1} & A_{R-\lambda_1} & A_{T-\lambda_1} \\ 1 & \frac{1}{\lambda_2^2} & A_{E-\lambda_2} & A_{R-\lambda_2} & A_{T-\lambda_2} \\ 1 & \frac{1}{\lambda_{n-1}^2} & A_{E-\lambda_{n-1}} & A_{R-\lambda_{n-1}} & A_{T-\lambda_{n-1}} \\ 1 & \frac{1}{\lambda_n^2} & A_{E-\lambda_n} & A_{R-\lambda_n} & A_{T-\lambda_n} \end{bmatrix} \begin{bmatrix} c_0 \\ c_1 \\ c_2 \\ c_3 \\ c_4 \end{bmatrix} = \begin{bmatrix} A_{S-\lambda_1} \\ A_{S-\lambda_2} \\ A_{S-\lambda_{n-1}} \\ A_{S-\lambda_n} \end{bmatrix} \quad (8)$$

Column vectors  $\mathbf{1}$ ,  $\frac{1}{\lambda^2}$ ,  $\mathbf{A}_E$ ,  $\mathbf{A}_R$ ,  $\mathbf{A}_T$ ,  $\mathbf{c}$ , and  $\mathbf{A}_S$  are used to represent the different columns; the matrix in Eq. 8 can be expressed as

$$\begin{bmatrix} \mathbf{1} & \frac{1}{\lambda^2} & \mathbf{A}_E & \mathbf{A}_R & \mathbf{A}_T \end{bmatrix} \mathbf{c} = \mathbf{A}_S \quad (9)$$

According to the least squares regression, the coefficients can be calculated by

$$\mathbf{c} = (\mathbf{V}^T \mathbf{V})^{-1} \mathbf{V}^T \mathbf{A}_S \quad (10)$$

where  $\mathbf{V} = [\mathbf{1} \ \frac{1}{\lambda^2} \ \mathbf{A}_E \ \mathbf{A}_R \ \mathbf{A}_T]$ . The path lengths of the sample and the standard solution are often the same; thus, coefficient  $c_4$  is the target substance concentration ratio of the sample to the standard solution.

According to the definition of the quantitative detection limit proposed by Currie,<sup>9</sup> the target substance can reliably be quantified when the selectivity of the target substance is  $> 10$ ; the selectivity  $SEL$  can then be calculated as

$$SEL = \frac{\|(\mathbf{I}_{n \times n} - \mathbf{U} \times \mathbf{U}^+) \mathbf{A}_{target}\|}{\|\mathbf{A}_{target}\|/r} \quad (11)$$

where,  $\mathbf{U} = [\mathbf{1} \ \frac{1}{\lambda^2} \ \mathbf{A}_E \ \mathbf{A}_R]$ ,  $\mathbf{U}^+$  is the Moore–Penrose pseudoinverse of the matrix,  $\mathbf{A}_{target}$  is the absorption spectra of the target substance, and  $r$  is the relative error of the instrument. For the UV–Vis spectrum, the relative error of the standard spectrum can generally be set to 2%.<sup>10</sup>

Based on error-delivering theory, the relative error of the concentration of the target substance originates from two sources: the relative measurement errors of the sample and the standard solution. The relative error can be calculated by the following formula:

$$\Delta c/c = \frac{\|\mathbf{x}^*\|/(\mathbf{x}^{*t} \mathbf{y}^*) R_s + \|\mathbf{x}^*\|/(\mathbf{x}^{*t} \mathbf{x}^*) R_t}{\|\mathbf{x}^*\|/(\mathbf{x}^{*t} \mathbf{y}^*) R_s + \|\mathbf{x}^*\|/(\mathbf{x}^{*t} \mathbf{x}^*) R_t} \quad (12)$$

where

$$\begin{aligned} \mathbf{x}^* &= (\mathbf{I}_{n \times n} - \mathbf{U} \times \mathbf{U}^+) \mathbf{A}_T, \\ \mathbf{y}^* &= (\mathbf{I}_{n \times n} - \mathbf{U} \times \mathbf{U}^+) \mathbf{A}_S, R_s, \text{ and } R_t \end{aligned}$$

are the relative measurement errors of the sample and the standard solution.

## Experimental

We designed an experiment to verify the performance of the proposed method for eliminating the influence of rough surfaces on quantitative analysis by absorption spectroscopy.

### Reagents and Apparatus

Orange gelb (Orange G; CAS: 1936-15-8) was chosen as the target substance because of its good light fastness, and deionized water was used as the solvent. Cuvettes (catalog no. 14-955-130) with a light path of 10 mm were purchased from Fisher Scientific.

A Form Talysurf (FTS-Intra) 1.30 (Taylor Hobson) surface-roughness measurement instrument was used to obtain the RMS roughness of the surfaces. A Lambda 850 (PerkinElmer) UV–Vis spectrophotometer was used to carry out spectrophotometric analyses in the wavelength range from 380 to 550 nm at every 1 nm. The selectivity was calculated to be 11.34. The target substance (Orange G) could be reliably quantified.

### Procedure

Solutions with five different concentrations (1 mmol/L, 0.75 mmol/L, 0.5 mmol/L, 0.25 mmol/L, and 0.05 mmol/L) were prepared by dissolving Orange G in deionized water. The cuvettes used in the experiment, which are numbered 1–13, are shown in Fig. 3a.

Ten cuvettes with different surface qualities were prepared by polishing the two outer transmission surfaces (surfaces 1 and 2, as shown in Fig. 3b). The transmittances

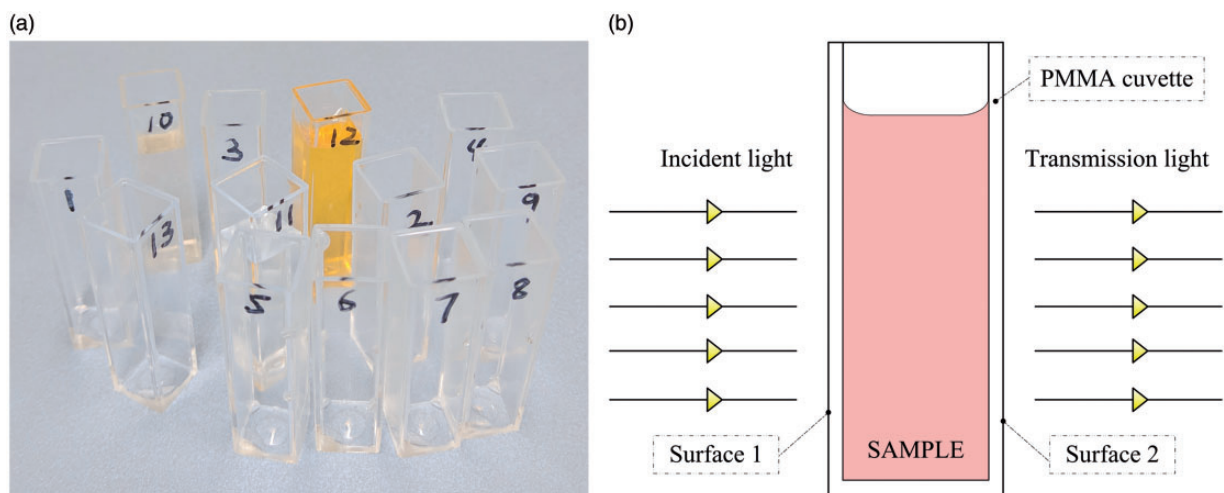


**Figure 3.** (a) Cuvettes used in the experiment. (b) Illustration of surfaces 1 and 2.

**Table 1.** Transmittances of the cuvettes filled with water at a wavelength of 440 nm and the outer transmission surface roughness of these cuvettes.

Cuvette no.	Transmittance (%)	Surface 1 (nm)	Surface 2 (nm)
1	87.22	57.4	43.7
2	84.68	62.4	62.5
3	81.69	77.3	75.2
4	79.05	42.2	41.4
5	76.30	61.6	105.8
6	73.66	117.3	122
7	69.84	176.8	156.2
8	64.55	179.4	205.9
9	62.63	161.6	254.2
10	66.55	138.8	137.2
11	91.69	33.2	31.3
12	90.59	40.9	38.9
13	91.48	31.3	37.3

of the cuvettes filled with water at a wavelength of 440 nm and the outer transmission surface roughness of these cuvettes are listed in Table 1.

All of the absorption spectra were measured relative to air.  $A_E$  and  $A_R$  were obtained with cuvette 12 when it was empty and filled with water, respectively.  $A_T$  was measured with cuvette 13 filled with 0.5 mmol/L Orange G solution used as the standard solution. Cuvettes 1–11 are sample cells. The samples were water and solutions with five different concentrations. Parts of the absorption spectra ( $A_{S}$ ) are shown in Figs. 4 and 5.

The spectra ( $A_E$ ,  $A_R$ ,  $A_T$ ,  $A_S$ ) and wavelength values were substituted into Eq. 10 to calculate the concentration ratio of Orange G relative to 0.5 mmol/L.

### Results and Discussion

As shown in Table 1, the surface roughness is as high as 250 nm; thus, the surface quality requirement class is B3 according to the SPI polishing standard, which is easily achieved. Moreover, the surface quality range of the 11 sample cuvettes covers most of the actual situations that may occur during injection molding. The transmittance differences between cuvettes 1–11 (used as sample cells) and cuvette 12 (used as a reference cell) are in the range of 1.1–28%. The light intensity reduction is less than an order of magnitude; thus, the signal-to-noise reduction is not obvious. The cuvette transmittances are greatly influenced by their surface quality. Furthermore, the transmittances are not perfectly correlated with the roughness of the surfaces because part of the scattering light is coincident with the transmission light, entering the detector at the same time. When the surface roughness is the same, a longer autocovariance length results in more scattering light entering the detector.<sup>11</sup> For the same reason, the measured transmittance is greater than the value calculated by Eq. 2. However, this scenario only affects the magnitude of the coefficients  $c_0$  and  $c_1$  in this method. It was ignored during the formula derivation because we focused only on coefficient  $c_4$ .

The true values of the concentration ratio were obtained from the absorbance of Orange G in five solutions with different concentrations at a wavelength of 479 nm, as measured by the standard method. Table II shows that the deviation of the predicted value is < 1.5%; this deviation calculated by Eq. 12 is 1.43%. The CVs of the concentration ratios of each concentration from the multiwavelength

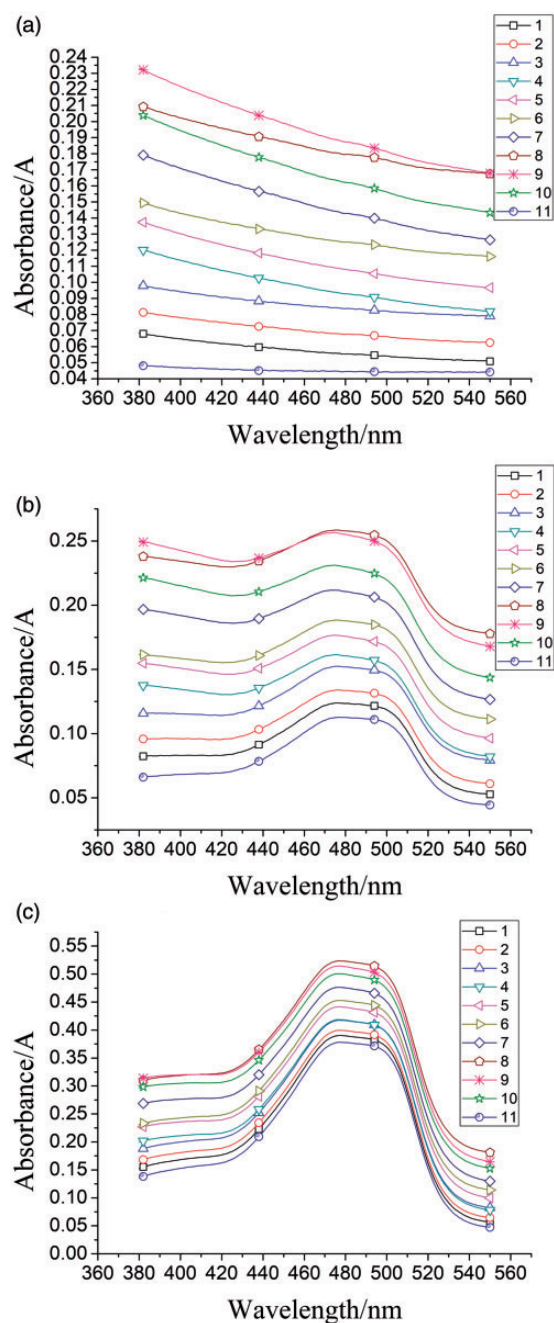


**Figure 4.** Absorption spectra of solutions with different concentrations in different cuvettes (nos. 1–11); (a), (b), and (c) are the spectra of the 11 sample cuvettes filled with water and 0.05 mmol/L and 0.25 mmol/L Orange G solution, respectively.

model are  $< 1\%$ . However, in the same situation, the worst CV could reach 28.2% by traditional single wavelength measurement. In the proposed model, the  $R^2$  statistics of multiple linear regression of the samples are all  $> 0.999$ , which means the model is consistent with the actual condition.

In the traditional double-wavelength method, the light intensity losses caused by surfaces at different wavelengths

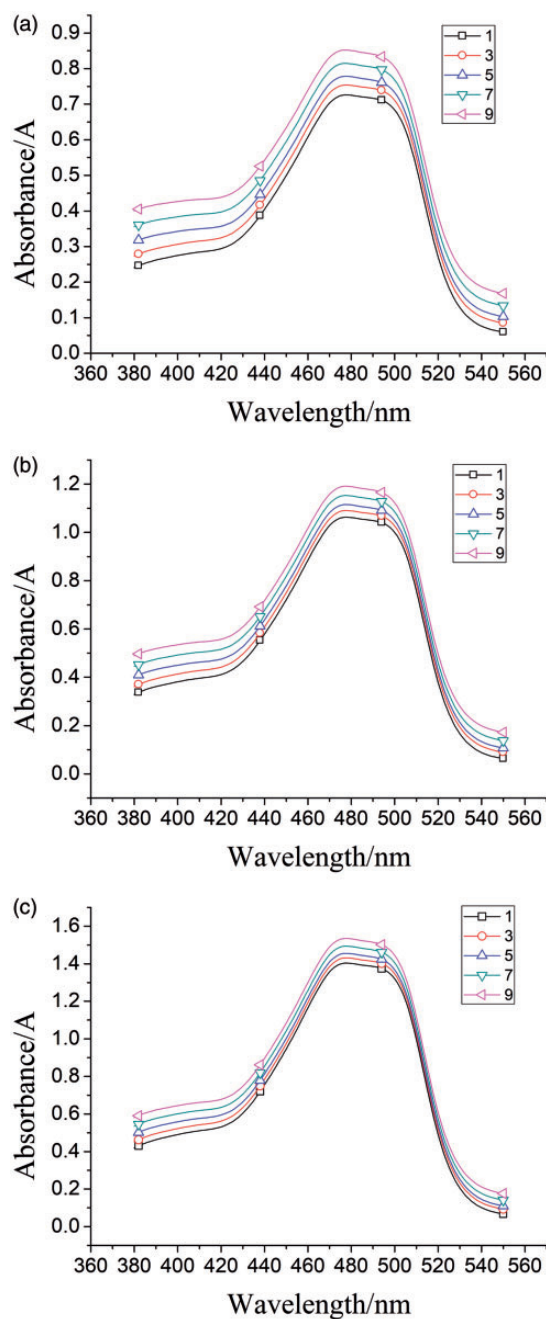


**Figure 5.** Absorption spectra of solutions with different concentrations in different cuvettes (nos. 1, 3, 5, 7, and 9); (a), (b), and (c) are the spectra of the five sample cuvettes filled with 0.5 mmol/L, 0.75 mmol/L, and 1 mmol/L Orange G solution, respectively.

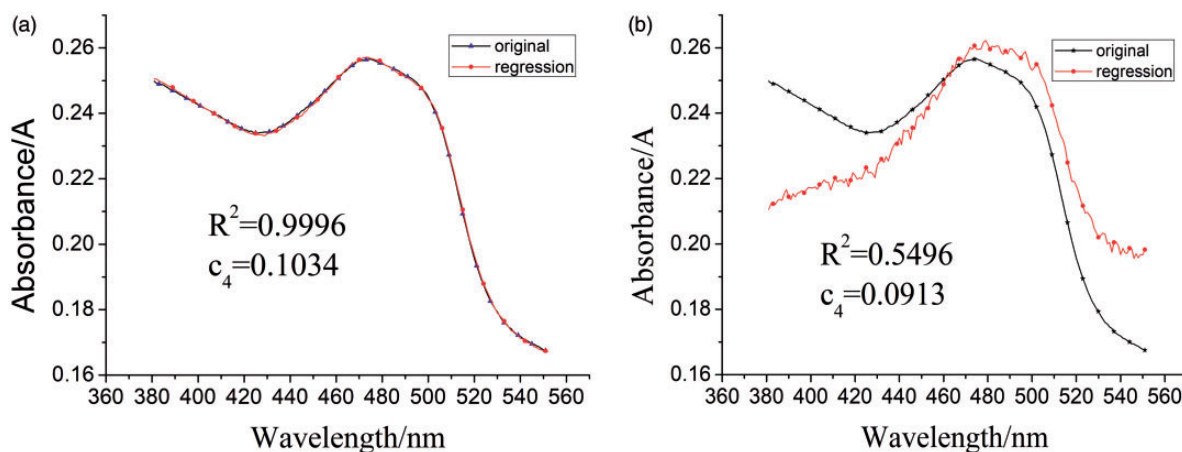
are considered to be the same. In this experiment, the sample chamber absorbance is

$$\left[ \mathbf{1} \quad \mathbf{A}_E - d_1^c \frac{\mathbf{1}}{\lambda^2} \quad \mathbf{A}_R - d_1^c \frac{\mathbf{1}}{\lambda^2} \quad \mathbf{A}_T \right] \mathbf{c} = \mathbf{A}_S \quad (13)$$

where  $d_1^c$  and  $d_1^t$  are the coefficients of  $\mathbf{A}_E = d_0^c \mathbf{1} + d_1^c \frac{\mathbf{1}}{\lambda^2}$  and  $\mathbf{A}_R = d_0^t \mathbf{1} + d_1^t \frac{\mathbf{1}}{\lambda^2}$  calculated using least squares

**Table II. Concentration ratios of Orange G calculated by the proposed model and the relative deviations of them from the true values.**

Category	0.05 mmol/L		0.25 mmol/L		0.5 mmol/L		0.75 mmol/L		1 mmol/L	
	Ratio	Deviation (%)	Ratio	Deviation (%)	Ratio	Deviation (%)	Ratio	Deviation (%)	Ratio	Deviation (%)
True value	0.1024		0.4980		1		1.4994		2.0020	
1	0.1027	0.3	0.4993	0.3	1.0006	0.1	1.5039	0.3	2.0105	0.4
2	0.1027	0.3	0.4982	0	0.9992	-0.1	1.5004	0.1	2.0061	0.2
3	0.1022	-0.2	0.4979	0	1.0006	0.1	1.5020	0.2	2.0089	0.3
4	0.1024	0.0	0.4971	-0.2	0.9999	0	1.4998	0	2.0035	0.1
5	0.1022	-0.2	0.4969	-0.2	1.0008	0.1	1.5019	0.2	2.0079	0.3
6	0.1025	0.1	0.4970	-0.2	1.0010	0.1	1.5038	0.3	2.0100	0.4
7	0.1037	1.3	0.4984	0.1	1.0032	0.3	1.5065	0.5	2.0139	0.6
8	0.1029	0.5	0.4979	0.0	1.0030	0.3	1.5067	0.5	2.0167	0.7
9	0.1034	1.0	0.4983	0.1	1.0033	0.3	1.5081	0.6	2.0192	0.9
10	0.1032	0.8	0.4968	-0.2	0.9998	0	1.5036	0.3	2.0152	0.7
11	0.1018	-0.6	0.4984	0.1	1.0010	0.1	1.5061	0.4	2.0210	0.9
Average	0.1027		0.4978		1.0011		1.5039		2.0121	
CV	0.54%		0.16%		0.14%		0.18%		0.28%	

**Figure 6.** Results of multiple linear regression for cuvette 9 filled with 0.05 mmol/L Orange G solution: (a) regression with Eq. 9; (b) regression with Eq. 13 and not considering the wavelength-dependent changes in scattering.

regression, respectively; as the molar absorptivities of PMMA and the reference solution are approximately constant in the wavelength range of 380–550 nm.

When the concentration ratios of Orange G are calculated by Eq. 13 via least squares regression, the CV reaches 3.57% and the deviation reaches -10.8% in the worst case. The model of Eq. 13 fits the measurement data worse. Taking cuvette 9 filled with 0.05 mmol/L solution as an example, the regression results obtained with Eq. 9 and Eq. 13 are shown in Fig. 6. The  $R^2$  value is reduced to 0.5496 from 0.9996.

The concentration ratios (calculated by different methods) were compared with their true values for the data corresponding to cuvette 9 filled with 0.05 mmol/L solution, cuvette

7 filled with 0.25 mmol/L solution, cuvette 5 filled with 0.5 mmol/L solution, cuvette 3 filled with 0.75 mmol/L solution, and cuvette 1 filled with 1 mmol/L solution. The original data and the linear fitting results are shown in Fig. 7. The slope of the linear fit of the values calculated by the model proposed in this work is closest to 1 and the intercept is closest to 0.

Taking air as a reference ensures the accuracy of the spectral measurements that are not influenced by the absorption cell difference because air does not require the cell to be contained. In a microchip system, multiwavelength spectra can be measured using a xenon lamp as a polychromatic light source and a charge-coupled device or photodiode array as the detector; thus, this approach is practicable.

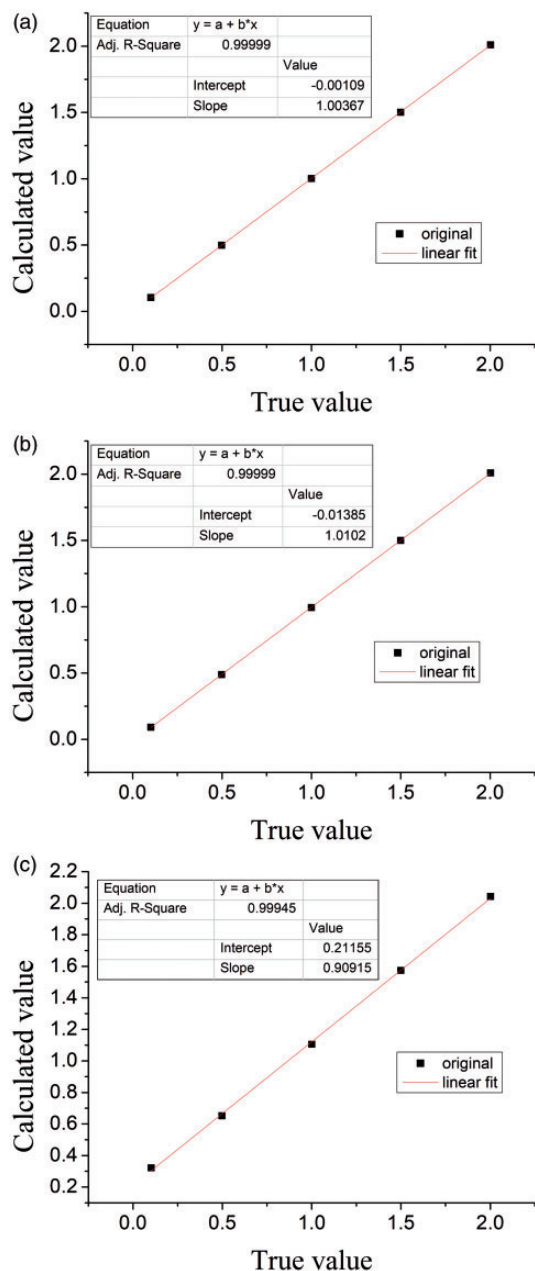


**Figure 7.** Comparison between the concentration ratios (calculated by different methods) and their true values: (a) calculated using the model of Eq. 9, (b) calculated with the model of Eq. 13, and (c) calculated with the absorbance at the wavelength of 479 nm measured using the traditional single-wavelength double-beam method.

## Conclusion

An alternative method for the quantitative determination of the targets (with known chemical components) on a

centrifugal microfluidic chip was proposed. The effect of interface scattering on spectrophotometry was eliminated by our multiwavelength linear model. As shown in the experiments, the accuracy and precision of the measurements are guaranteed when the transmittance difference is  $\leq 20\%$ . The surface quality requirement of the injection molding of the chip can be greatly reduced. Manufacturing difficulties will be greatly reduced for the proposed high-throughput chips. We expect applications involving microfluidic chips to greatly benefit from this technology.

## Conflict of Interest

The authors report there are no conflicts of interest.

## Funding

This research was funded by the National Major Scientific Instrument Development (61727813), the Chinese Academy of Sciences\_WeiGao Research and Development Plan (2017010), and the Jilin Province Development and Reform Commission (2015Y028).

## ORCID iD

Yang Xu  <http://orcid.org/0000-0001-5449-7460>

Mingbo Chi  <http://orcid.org/0000-0001-8683-4257>

## References

1. R. Gorkin, J. Park, J. Siegrist, M. Amasia, et al. "Centrifugal Microfluidics for Biomedical Application". *Lab on a Chip*. 2010. 10(14): 1758–1773.
2. C. Schembri, T. Burd, A. Kopf-Sill, L. Shea, et al. "Centrifugation and Capillarity Integrated into a Multiple Analyte Whole Blood Analyzer". *J. Anal. Methods Chem.* 1995. 17(3): 99–104.
3. B.S. Lee, J.-N. Lee, J.-M. Park, J.-G. Lee, et al. "A Fully Automated Immunoassay from Whole Blood on a Disc". *Lab on a Chip*. 2009. 9(11): 1548–1555.
4. N.M.M. Pires, T. Dong, U. Hanke, N. Hoivik. "Recent Developments in Optical Detection Technologies in Lab-on-a-Chip Devices for Biosensing Applications". *Sensors*. 2014. 14(8): 15458–15479.
5. T. Bauer. "Insert Quality and Molded Parts". In: S. Bäumer, editor. *Handbook of Plastic Optics*. Weinheim: John Wiley and Sons, 2011.
6. H.E. Bennett. "Scattering Characteristics of Optical Materials". *Opt. Eng.* 1978. 17(5): 175480.
7. J. Ebert, H. Pannhorst, H. Küster, H. Welling. "Scatter Losses of Broadband Interference Coatings". *Appl. Opt.* 1979. 18(6): 818–822.
8. C. Carniglia. "Scalar Scattering Theory for Multilayer Optical Coatings". *Opt. Eng.* 1979. 18(2): 104–115.
9. L.A. Currie. "Limits for Qualitative Detection and Quantitative Determination. Application to Radiochemistry". *Anal. Chem.* 1968. 40(3): 586–593.
10. F. Zscheile Jr, H.C. Murray, G. Baker, R. Peddicord. "Instability of Linear Systems Derived from Spectrophotometric Analysis of Multicomponent Systems". *Anal. Chem.* 1962. 34(13): 1776–1780.
11. J. Elson, J. Rahn, J. Bennett. "Relationship of the Total Integrated Scattering from Multilayer-Coated Optics to Angle of Incidence, Polarization, Correlation Length, and Roughness Cross-Correlation Properties". *Appl. Opt.* 1983. 22(20): 3207–3219.